ATOMIC COLLISION PROCESSES RELATING TO THE IONOSPHERE*

Sponsored by Advanced Research Projects Agency

FINAL REPORT

Period of Report: September 1, 1969 - August 31, 1970
Effective Date of Contract: June 30, 1969
Period of Contract: September 1, 1969 - August 31, 1970

ARPA Order Number: ARPA 1482
Contract Number: DAHC04-69-C-0094
Program Code Number: 9E20

Principal Investigators and Project Scientists: P. J. Chantry (412) 256-3675
A. V. Phelps†

†Present address: Joint Institute for Laboratory Astrophysics, Boulder, Colorado

Arc and Plasma Research
Westinghouse Research Laboratories
Pittsburgh, Pennsylvania 15235

ATOMIC COLLISION PROCESSES RELATING TO THE IONOSPHERE*

Sponsored by Advanced Research Projects Agency

FINAL REPORT

Period of Report: September 1, 1969 - August 31, 1970
Effective Date of Contract: June 30, 1969
Period of Contract: September 1, 1969 - August 31, 1970

ARPA Order Number: ARPA 1482
Contract Number: DAHC04-69-C-0094
Program Code Number: 9E20

Principal Investigators and Project Scientists: P. J. Chantry (412) 256-3675
A. V. Phelps†

†Present address: Joint Institute for Laboratory Astrophysics, Boulder, Colorado

Arc and Plasma Research
Westinghouse Research Laboratories
Pittsburgh, Pennsylvania 15235

ABSTRACT

This final report is an account of work performed under Contract DAHC04-69-C-0094 during the total period of the contract, September 1, 1969 - August 31, 1970. Measurements of the attachment cross-sections in O_3 reveal no dependence on temperature below 360°K in the energy range 0-4 eV. The peak value of the total attachment cross-section Q_a, of $(3.0 \pm \frac{0.7}{0.4}) \times 10^{-17}$ cm^2 occurs at an electron energy of 1.07 eV. The individual cross-sections for production of O^- and O_2^- peak at energies of 1.25 eV and 0.95 eV respectively. The ratios of the three cross-sections Q_a:$Q(O^-)$: $Q(O_2^-)$ at their peaks are 1.6:1:0.75. A discrepancy at electron energies above 1.5 eV between the measured sums of $Q(O^-) + Q(O_2^-)$ and Q_a is ascribed to high kinetic energy O_2^- and O^- ions. From the measured onset for O_2^- production a value of $A(O_2) \geq 0.60 \pm \frac{0.05}{0.15}$ eV is deduced for the electron affinity of O_2. Measurements are presented of the momentum transfer cross-section in N_2 in the range of energy 1-20 eV, and reasons advanced why these must be regarded as lower limits at this time. Measurements of a quantity $Q_g \approx (Q_m \Sigma Q_x)^{1/2}$ in N_2 and O_2 between approximately 10 and 20 eV are presented. Using literature values of Q_m the measured quantity Q_g yields the electron energy dependence of ΣQ_x, the total inelastic collision cross-section. Preliminary measurements of the attachment of low energy electrons to SF_4 are also presented.

TABLE OF CONTENTS

BLANK PAGE

1. INTRODUCTION

This final report contains an account of work performed under Contract DAHC04-69-C-0094, ARPA Order No. 1482, administered by the Army Research Office, Durham, and covers the total period of the contract, September 1, 1969, to August 31, 1970. Progress during the first seven months of this period was previously reported in detail in the Annual Report[1] on this contract. For completeness much of the data reported therein is reproduced here. Where this is the case the discussion of experimental detail has been appropriately condensed.

The experimental work described herein was performed by P. J. Chantry, except that of section 2.2 which was performed by C. L. Chen in collaboration with P. J. Chantry. Up to the time of his departure from Westinghouse Research Laboratories in June of 1970, A. V. Phelps participated in the planning and interpretation of the experiments.

---

1) Annual Report, Contract DAHC04-69-C-0094, submitted April, 1970.

2. TECHNICAL ACCOMPLISHMENTS

2.1 ELECTRON ATTACHMENT IN OZONE

The details of the apparatus and experimental methods used in this study have been previously described.[1] For completeness they are briefly reviewed below and, in addition, some previously unreported data is presented.

2.1.1 Experiment

The ozone used in the present work was made by flowing the products of a microwave discharge in oxygen through a liquid nitrogen trap, which served to collect the ozone. Ten minutes' operation of this system sufficed to produce enough ozone for a day's operation of the experiment. The ozone was admitted to the collision chamber through the tube shown in Fig. 1. The pressure of ozone in the collision chamber was measured by a Baratron[2] gauge connected separately into the chamber, and controlled by varying the temperature of the ozone reservoir by using various ratios of liquid nitrogen to oxygen in the reservoir trap.

The temperature of the ozone in the collision chamber was controlled by the use of various fluids in the trap shown in Fig. 1. Precooling (or heating) of the ozone was achieved by its passage through the stainless steel gas inlet tube which passed down the center of the trap, as shown. The temperature of the gas in the collision chamber was assumed to be the mean of the temperatures indicated by thermocouples situated at the bottom of the trap and at the base of the collision

---

2) MKS Instruments, Burlington, Mass.

chamber. This assumption was substantiated, at least in so far as the translational temperature is concerned, by measurements[1] of the total positive ion current versus Baratron pressure reading.

2.1.2 Results

The total attachment cross-section, indicated by Q_a in Fig. 2, was obtained by measuring the "total" ion current reaching the "attractor" electrode as a function of electron energy and comparing the result with similar measurements on gases for which the cross-section is known. The peak total attachment cross-section of $(3.0 \pm 0.7) \times 10^{-17}$ cm^2 occurs at 1.07 eV.

The total attachment cross-section arises from two reactions

$$e + O_3 \rightarrow O^- + O_2 \qquad (1)$$

and

$$e + O_3 \rightarrow O_2^- + O \qquad (2)$$

The individual cross-sections for these, shown in Fig. 2, were obtained from mass-spectrometric and ion energy analysis of the sample of ions leaving the collision chamber through the slit in the attractor. The contribution of the O^- cross-section to the total was determined by using mixtures of O_3 and CO_2 and comparing the detected total and O^- signals over the energy range 0 - 6 eV. The assumption that the sensitivity of the system to O^- from O_3 was the same as that for O^- from CO_2 was based on the observed close similarity of the O^- kinetic energy spectra at the cross-section peaks. The contribution of the O_2^- cross-section to the total was determined by establishing that the bulk of the O_2^- ions are formed with very little kinetic energy, irrespective of the electron energy in the range shown in Fig. 2. Thus, the mass-analyzed O_2^- signal was assumed to have the same shape as the true cross-section. Its magnitude was adjusted to give agreement

between the sum of the O^- and O_2^- cross-sections and the measured total. It is gratifying that the above procedure was completely self-consistent between 0 and 1.5 eV, as shown by the full Q_a curve and the broken curve in Fig. 2.

The cross-sections for O^- and O_2^- peak at 1.25 eV and 0.95 eV, respectively. The ratios of the three cross-sections Q(total): $Q(O^-)$: $Q(O_2^-)$ at their peaks are 1.6:1:0.75.

The discrepancy between the sum $Q(O^-) + Q(O_2^-)$, indicated by the broken curve, and Q_a is accounted for, at least in part, by negative ions produced with sufficient kinetic energy to preclude their detection when the Wien filter, mass-spectrometer system was set to detect the predominant zero energy ion peaks. The presence of such ions is shown in Fig. 3, where O^- kinetic energy spectra are shown for four values of the electron energy. All curves have been normalized to the same zero-energy peak height. At electron energies below approximately 1.5 eV, only the zero-energy peak is detected. This peak persists throughout the electron energy range shown, but, in addition, there is a second peak of higher kinetic energy where position varies with the electron energy.

O_2^- is found to behave similarly in that, at electron energies of ~3 eV and above a high kinetic energy peak appears in addition to the zero energy peak, which persists throughout this range. The signal, however, is approximately a factor of 30 lower than the O^- signal. The behavior of both peaks is shown in Fig. 4, where their positions are plotted as a function of electron energy.

When dissociative attachment leads to one or more molecular fragments, as in this case, the most probable ion kinetic energy can be predicted only to the extent that it cannot exceed the amount

$$E_o = (1 - \beta)\{V_e - (D - A)\} \qquad (3)$$

where β is the ratio of the ions mass to the mass of the parent molecule, V_e is the electron energy, D is the strength of the broken bond, and A is the electron affinity. Thus, Eq. 3 results from energy and momentum conservation and applies only when no energy is converted to internal excitation, vibrational and/or rotational, of the molecular fragment. Equation 3 is indicated in Fig. 4 by the broken lines, the values of the constants[3,4,5] used being D = 1.00 eV, $A(O^-)$ = 1.47 eV, and $A(O_2^-)$ = 0.43 eV. We note that in both cases the data points lie below the broken lines, showing that significant amounts of energy are carried away as vibrational or rotational excitation.

A puzzling feature of the O^- data points in Fig. 4 is that they lie very close to the full line shown whose slope is 1/2. No explanation of this effect can be offered at this time. Most of the O_2^- data points, on the other hand, behave essentially according to Eq. 3 with A = 0, and are therefore consistent with the assumption that the O_2^- ions produced by this particular process are formed predominantly in the highest vibrational state which is stable against auto-detachment.

The cross-sections shown in Fig. 2 were found to be insensitive to gas temperature between 112° and 360°K. Particular attention was paid to the threshold regions where any dependence on temperature is likely to be most pronounced.[6] None, however, was observed. It therefore appears that the threshold measured for O_2^- production should provide a valid upper limit estimate for $D-A(O_2)$, hence, a lower limit to $A(O_2)$. The result from the present work, $A(O_2) \geq 0.60 \begin{matrix} + 0.05 \\ - 0.15 \end{matrix}$ eV, is

---

3) G. Herzberg, Molecular Spectra and Molecular Structure III. (D. Van Nostrand, Inc., New York, 1966).

4) L. M. Branscomb, D. S. Burch, S. J. Smith, and S. Geltman, Phys. Rev. 111 504 (1958).

5) J. L. Pack and A. V. Phelps, J. Chem. Phys. 44, 870, 1966.

6) P. J. Chantry, J. Chem. Phys. 51 3369 (1969).

in excellent agreement with the previous work by Curran[7] in which no attempt was made to control the gas temperature.

The magnitude and shape of the total attachment cross-section shown in Fig. 2, and its insensitivity to temperature, are consistent above 0.3 eV with the swarm measurements of attachment coefficient by Stelman and Phelps.[8] Below 0.2 eV, however, their data requires a cross-section significantly smaller than that found in the present measurements, and increasing approximately linearly with electron energy. Such a cross-section is shown by the broken curve at energies below 0.5 eV in Fig. 2. In total collection measurements such as were used in the present study there always exists the possibility that scattered electrons are being collected, particularly at low impact energies. The shape of the total curve at these energies is substantiated in this case, however, by the measured O^- cross-section where there can be no contribution from scattered electrons. No explanation of the low energy discrepancy between the present data and the swarm data can be offered at this time.

---

7) R. K. Curran, J. Chem. Phys. 35, 1849 (1961).

8) D. Stelman and A. V. Phelps, Final Report, Contract F29601-68-C-0070, June, 1969.

2.2 ELECTRON ATTACHMENT TO SF_4

In the early stages of its thermal decomposition SF_6 gives predominantly SF_4 and F over a fairly wide range of temperature.[9] Hence, some of the effects of elevated temperature on the production of negative ions[10] from SF_6 could be ascribed to attachment to "hot" SF_6 molecules or to attachment to SF_4 molecules created by thermal dissociation. If, on the other hand, one knew the attaching properties of SF_4 as a function of gas temperature, then it should be possible to resolve such questions as the above and predict the attaching properties of mixtures, in particular, equilibrium mixtures of SF_6 and SF_4. To this end measurements were initiated in the same apparatus used previously[6,10] to study N_2O and SF_6 at elevated temperatures. The results obtained in the brief time available for this work are summarized below.

SF_4 was used directly as obtained from the supplier[11] and contained 5-9% SOF_2 and <0.3% Cl_2 as impurities. It was admitted to the collision chamber either alone or mixed with SF_6, the latter being present for electron energy scale calibration and comparison of ion signal strengths.

The SF_4^- and SF_3^- signals detected at room temperature with low energy electrons are shown in Fig. 5. At energies very close to zero SF_4^- ions are observed, the width of the peak being controlled by the available electron energy resolution (0.08 eV FWHM). A similar, though much smaller peak is observed for SF_3^-, and in addition a much broader

---

9) R. L. Wilkins, J. Chem. Phys. 51, 853 (1969).

10) C. L. Chen and P. J. Chantry, Bull Amer. Phys. Soc. II 15, 418 (1970). See also Final Report, Contract N00014-68-C-0490, Sept., 1969.

11) Matheson Company Inc., East Rutherford, New Jersey.

peak is centered at about 1.4 eV. Note that in Fig. 5 the SF_4^- signal has been scaled down by 10^{-3} in order to show it with the SF_3^- signal.

Using an equal parts mixture of SF_6 and SF_4 the ratio of the SF_6^- : SF_4^- signals at zero energy was found to be 10 at room temperature. This ratio cannot be assumed to represent the ratio of the attachment cross-sections because of the following unknown factors: relative sensitivities of the high pressure gauge, used to monitor the collision chamber pressure, to SF_6 and SF_4; relative effects on the signal levels of the decay of SF_6^- and SF_4^- by auto-detachment during their collection time; relative collection efficiencies for the two ions.

Raising the gas temperature has the effect of decreasing the SF_4^- peak signal while the SF_3^- peak increases in magnitude and shifts to lower energy.

In addition to the above ions F^- is also detected in the energy range of Fig. 5. At room temperature it peaks at approximately 0.7 eV, the peak signal being approximately one third the SF_4^- peak. Raising the temperature introduces an F^- peak at essentially zero energy which becomes the predominant ion formed with low energy electrons (<0.1 eV) at high temperature. Unfortunately there was insufficient time to confirm that the F^- signal does not come from the SOF_2 impurity rather than the SF_4.

2.3 TOTAL INELASTIC COLLISION CROSS-SECTIONS

The present experiment was developed specifically for the measurement of the momentum transfer cross-section and the total inelastic collision cross-section. The design of the experiment and quantitative interpretation of the results relies heavily on previously published theoretical work[12] on the behavior of a mono-energetic electron beam injected into a gas at intermediate and high gas pressures where the mean free path for scattering is comparable to or much smaller than the collision chamber length. The theory assumes that the electrons can suffer either elastic collisions or "absorbing" collisions. The latter are assumed to remove the electron from the system. From a practical viewpoint "absorbing" collisions may be made to correspond to any inelastic collision which decreases the electron's energy below the threshold of the process used to detect them. In the present experiment this process is positive (or negative) ion production. Hence the present technique may be used to study the total inelastic collision cross-section at electron energies in the range from the threshold ε_T to $\varepsilon_T + \varepsilon_1^*$ where ε_1^* is the lowest relevant excitation energy.

In what follows we describe under separate headings the experimental apparatus and procedure, the theory through which the data is interpreted, and the results obtained.

2.3.1 Experiment

The apparatus employed in the present study is shown in Fig. 6. The electrode system is shown approximately to scale; the vacuum system is only schematic. The separation of the entrance and exit grids is 10 cm.

---

12) P. J. Chantry, A. V. Phelps, and G. J. Schulz, Phys. Rev. 152, 81 (1966).

The electron beam is produced from a thoria-coated iridium filament, collimated by the electrodes shown and enters the collision chamber through a 0.020" diameter aperture in the Entrance Plate. The beam is aligned by a magnetic field of 700 gauss whose direction relative to the tube axis is adjusted to give maximum electron current to electron collector 2 when the tube is at low pressure. Thereafter, the two electron collectors are connected together and the total current to both is monitored. The pressure in the collision chamber is controlled by variable leak valves backed by high pressure cylinders of research grade gases. Frequently, mixtures of two gases are employed. The total pressure in the collision chamber is monitored by a Baratron[2] absolute pressure gauge.

Two distinct type of measurement are made with this system. The fraction of the injected electron current reaching the upper end of the chamber, where it is collected primarily by EC_1 and EC_2, is measured as a function of pressure and electron energy. In so doing an effort is made to insure that scattered electrons approaching the entrance plate and electron collectors are absorbed rather than reflected at these boundaries. To this end a small accelerating voltage of one or two volts is applied between the entrance grid and the entrance plate, and similarly between the exit grid and the electron collectors. In addition the entrance plate and electron collectors are plated with "platinum black." All other electrodes are gold plated. In these particular measurements, of the transmitted electron current, there is in principle no need for a transverse electric field across the parallel plates which define the potential of the collision chamber. Such a field is, however, applied in an effort to prevent the escape from the collision chamber of back-scattered electrons through the aperture in the entrance plate. An electron which escapes in this way is expected to be ultimately reflected back into the collision chamber by the field which serves to accelerate the electrons from the filament to the collision chamber. In the presence of the crossed E and B fields in the collision chamber all electrons suffer a transverse drift motion with velocity $v = E/B$, and

the hope is that an electron back-scattered to the entrance plate will have drifted transversely a sufficient distance to miss the aperture and hit the plate.

In addition to the measurements of transmitted electron current the spatial variation of electron density in the chamber is measured as a function of electron energy and pressure by monitoring the ion currents arriving at the collectors $C_{1,2\&3}$. These collector plates are situated behind mesh covered apertures in the otherwise continuous plate. The sizes of these apertures and their positions relative to the entrance plate are accurately known for purposes of comparision with the theory. The relative sizes of the apertures were chosen to provide comparable currents to all three collectors over as large a range of pressure as possible. Thus, at low pressures the current to C_3 exceeds that to C_1 by a factor of approximately 20 due to the different aperture sizes. With increasing pressure the ratio of $I(C_1)/I(C_3)$ increases and can change by a factor of 400 without the currents differing in magnitude by more than a factor of 20.

Careful checks were performed to insure that the ratios of the ion currents $I(C_1):I(C_2):I(C_3)$ were constant over a reasonable range of the ion extraction field applied across the parallel plates and similarly regarding the effects of the accelerating voltage applied between $C_{1,2,3}$ and the adjacent plate. As a result of such checks the extraction voltage was chosen to be 20V, giving a field of 12.5 v/cm. In addition $C_{1,2,3}$ were kept 2V accelerating relative to the adjacent plate containing the mesh covered apertures.

2.3.2 Theory

The theory used in the analysis of the present experiment follows very closely that developed by Chantry, Phelps and Schulz.[12] The results presented in this reference are subject to two important restrictions: i) the elastic scattering was assumed isotropic, and ii) the equations derived become inaccurate if the total inelastic

collision cross-section ΣQ_x becomes comparable to the elastic scattering cross-section Q_e. For application to the present problem it is clearly desirable to remove both of these restrictions. We may approach the problem in three stages, as follows.

Conservative Anisotropic Scattering

The treatment developed in Ref. 12, while based on a two-stream approximation to the electron angular distribution, was shown to be equivalent to representing the transport of the scattered electrons by a diffusion mechanism. In view of this one intuitively expects that anisotropic elastic scattering may be taken into account in the theory by using the momentum transfer cross-section Q_m in place of the total elastic scattering cross-section Q_e. Justification for this may be found in the quantitative results of Orchard and Busbridge,[13] Orchard,[14] and van de Hulst and Grossman[15] who have calculated the transmission of photons through gases having various conservative anisotropic scattering phase functions. All the data may be shown to scale rather accurately if plotted as a function of the scattering depth, L, measured in units of the mean free path for momentum transfer, $(NQ_m)^{-1}$, rather the usual $(NQ_e)^{-1}$.

The procedure for analyzing the electron transmission data is therefore as follows. At fixed electron energy the fraction of the injected electron current which is transmitted to the electron collectors is plotted as a function of gas pressure on log-log paper. Using boundary conditions appropriate to the experiment, the theoretical transmission curve is calculated as a function of NQ_mL. By fitting the experimental

---

13) I. W. Busbridge and S. E. Orchard, Astrophys. J. 149, 655 (1967).

14) S. E. Orchard Astrophys J. 149, 665 (1967).

15) H. C. van de Hulst and K. Grossman, The Atmospheres of Venus and Mars, ed J. C. Brandt and M. B. McElroy, (Gordon and Breach, New York, 1968) p. 35.

to the theoretical curve, and converting the pressure scale to a gas density (N) scale, the value of Q_m is obtained at the electron energy used.

Non-Conservative Isotropic Scattering-Extension to ΣQ_x Comparable to Q_e

The problem of extending the range of applicability of the results of Ref. 12 to situations where ΣQ_x approaches Q_e in magnitude may be solved by replacing the variable q, defined in Ref. 12 as $NL\sqrt{3\Sigma Q_x(Q_e + \Sigma Q_x)}$ by a quantity S where for isotropic elastic scattering

$$S = kNL(Q_e + \Sigma Q_x) \tag{4}$$

$$k = \tanh\left(\frac{k}{\omega}\right) \tag{5}$$

$$\text{and } \omega = Q_e/(Q_e + \Sigma Q_x) \tag{6}$$

The parameter ω is adopted from the field of radiation transport[16] where it is called the albedo for single scattering. The parameter k is the "characteristic root,"[17] which is such that in an infinite medium, away from sources, the electron density varies as $\exp[-kN(Q_e + \Sigma Q_x)x]$. For values of ω close to unity it can be shown[18] that

$$k \simeq \sqrt{\omega(1 - \omega)} = \sqrt{3Q_e\Sigma Q_x}/(Q_e + \Sigma Q_x) \tag{7}$$

Hence,
$$S \simeq NL\sqrt{3Q_e\Sigma Q_x} \simeq q \tag{8}$$

---

16) See for example S. Chandrasekhar Radiative Transfer (Clarendon Press, Oxford, England, 1950).

17) See ref. 16, p. 19.

18) B. Davison, Neutron Transport Theory (Clarendon Press, Oxford, England, 1957), p. 55.

and we conclude that the more generally useful variable S define above is, in the limit of $\Sigma Q_x << Q_e$, equivalent to the variable q defined in Ref. 12.

Non-Conservative Anisotropic Scattering

The prescription for calculating k from ω (Eq. 5) is strictly applicable only to the case of isotropic scattering. The problem of non-conservative anisotropic scattering has been treated in some detail in Ref. 15 whose authors recommend that the effects of such a medium be calculated by replacing the anisotropic scatterers by centers having the same total inelastic scattering cross-section ΣQ_x, but which scatter isotropically with an elastic cross-section Q_e' of such a magnitude that the value of S obtained from Eq. 4 is appropriate to the true medium. A problem with this scaling law is that S, or equivalently k, must be independently estimated for the true medium by some reasonably accurate means. Provided $\Sigma Q_x << Q_e$ this may be done through the approximate relationship[19]

$$k = \sqrt{3Q_m \Sigma Q_x / (Q_e + \Sigma Q_x)} \qquad (9)$$

which when substituted into Eq. (4) gives

$$S = NL\sqrt{3Q_m \Sigma Q_x} \qquad (10)$$

We note that this is exactly the same result we would have obtained had we used Eq. 8 , but with Q_m replacing Q_e.

The procedure of replacing Q_e by Q_m and otherwise using the various equations applicable to isotropic scattering can, on the basis of the above discussion, clearly be regarded as equivalent to using van de Hulst's scaling laws,[15] provided we have $\Sigma Q_x << Q_e$. For ΣQ_x comparable to Q_e they are not equivalent. In addition to being much

---

19) J. E. Hansen, Astrophys. J. 158, 337 (1969).

simpler to apply the present procedure appears to be more accurate than that recommended by van de Hulst, at least in so far as can be judged from the data available in the literature, in particular in Ref. 15.

The presently adopted procedure may be formally stated as the following scaling law. "The transport of electrons through a medium which scatters anisotropically and "absorbs" electrons with a total inelastic scattering cross-section ΣQ_x may be obtained by treating the medium as an isotropic scatter having the same value of ΣQ_x, but with a total elastic cross-section equal to the momentum transfer cross-section Q_m of the true medium." Thus, for general use we rewrite Eqs. 4, 5, and 6 as

$$S = kNL(Q_m + \Sigma Q_x) \tag{11}$$

$$k = \tanh\left(\frac{k}{\omega}\right) \tag{12}$$

$$\omega = Q_m/(Q_m + \Sigma Q_x) \tag{13}$$

and when ω is close to unity

$$S \simeq NL\sqrt{3Q_m \Sigma Q_x} \tag{10}$$

The equations derived in Ref. 12 in terms of the quantities

$$q = NL[3(Q_e + \Sigma Q_x)\Sigma Q_x]^{1/2}$$

and $$m = Q_e/\Sigma Q_x$$

may without difficulty be rewritten in terms of the quantities S and ω. The solution for the spatial dependence of the electron density may then be integrated between limits appropriate to the extent of the apertures through which the ions pass to the collectors $C_{1,2,3}$ and the ratios of those integrals evaluated as functions of S with ω as parameter. At

sufficiently high values of S, which is proportional to pressure, the curves so obtained are rather insensitive to ω and the assumed boundary conditions. When S is in the region of unity the curves are somewhat sensitive to both ω and the boundary conditions, but it is difficult to identify which in any given practical case. Hence, the ion current ratio data permits a reasonably accurate determination of the proportionality constant relating S to the gas pressure, which according to Eq. 10 provides an approximate determination of $(Q_m \Sigma Q_x)^{1/2}$. The relationship may be made exact by the following procedure: Let us define a quantity Q_g, having the dimensions of a cross-section, by the equation

$$Q_g = S/\sqrt{3}\ NL \tag{14}$$

When $\Sigma Q_x << Q_m$ Eq. 10 gives

$$Q_g \simeq (Q_m \Sigma Q_x)^{1/2}$$

$$\Sigma Q_x \simeq Q_g^2/Q_m$$

Let us therefore, write, in general

$$\Sigma Q_x = \beta Q_g^2/Q_m \tag{15}$$

where $\beta \to 1$ for $\Sigma Q_x << Q_e$ and may otherwise be determined from the equation

$$\beta = \frac{3\omega(1-\omega)}{k^2} \tag{16}$$

obtained from Eqs. 12, 13, and 15. In addition we have from Eqs. 11 and 14 the equality

$$\frac{Q_g}{Q_m} = \frac{k}{\omega\sqrt{3}} \tag{17}$$

Since k is a function of ω alone we may compute β and Q_g/Q_m as functions of ω and plot β as a function of Q_g/Q_m. This has been done in Fig. 7 where in addition $\Sigma Q_x/Q_m$ has been plotted as a function of Q_g/Q_m.

The complete analysis of the data may then be achieved by
(i) comparing the measured and computed ion current ratios as functions of pressure and S respectively, and through Eq. 14 obtaining Q_g.
(ii) Provided Q_m is known the ratio Q_g/Q_m is calculated, the value of β read from Fig. 7, and the value of ΣQ_x than calculated from Eq. 15.

2.3.3 Results

Measurement of Q_m

These results have been previously reported[1] in some detail, including measurements on Xe as a test case. They are summarized below.

The pressure dependence of the fractional transmitted current has been shown to follow closely the shape predicted by the theory, allowing measurements of Q_m to be made more rapidly as a function of electron energy by using x-y plots of the transmitted current versus electron accelerating voltage at various fixed pressures.

The results directly relevant to the present study are those obtained in N_2, shown in Fig. 8. The discrepancy in this and other gases between the present data and that of previous workers has been found to be consistently in the direction expected if the electrons back-scattered to the entrance plate are partially reflected with a reflection coefficient which increases monotonically with electron energy. It has not been confirmed that this is the case, but until such an effect can be shown to be absent the present data must be assumed to provide only a lower limit to the true value of Q_m. Techniques for checking for and eliminating this effect have been suggested,[20] but there has been no opportunity to try them during the course of this contract.

---

20) P. J. Chantry, Proposal for continuation of Contract DAHC04-69-C-0094.

Attempts to measure the fractional transmitted current as a function of pressure and electron energy in O_2 were unsuccessful due to very serious pressure dependent "poisoning" of the filament by the oxygen.

Measurements of Q_g

An example of measurements of the various positive ion current ratios made in N_2 at an electron energy of 17 eV are shown in Fig. 9 by the points. The full curves are theoretical curves computed for $\omega = 0.9$ and for boundary conditions corresponding to no reflection of scattered electrons approaching the boundaries. It has been shown previously[1] that the theoretical curves plotted as a function of S are relatively insensitive to ω and the boundary conditions, particularly in the steeply rising region at the higher pressures. The lateral position of each computed curve in Fig. 9 has been adjusted for best fit to the appropriate set of data points. The vertical bar on each curve marks the position of S = 1, and the three sets of data are seen to give reasonable agreement as to the pressure p(1) at which S = 1. In this case $p(1) = (5.2 \pm 0.2) \times 10^{-3}$ Torr, which gives, via Eq. 14, $Q_g = 3.52 \times 10^{-16} cm^2$. The consistency observed between the three different ratios is an indication that the theory is predicting the forms of both the spatial and pressure dependencies of the electron density with reasonable accuracy.

In order to check that the dependence on pressure of the ion current ratios is indeed related to the inelastic collision cross-section similar measurements were made under conditions where $\Sigma Q \to 0$ An example of such data is shown in Fig. 10. The electron energy of 18 eV is well below the first excitation energy of He at 19.8 eV. In order to provide ionization for sensing the electron density a small partial pressure of NO was added to the He. It was demonstrated that the ratio $I^+(C_1)/I^+(C_3)$ was independent of the amount of NO present in the region of the low partial pressure employed. In this case, if the experiment were perfect, it would yield a curve consistent with $\omega = 1$ and $\Sigma Q_x \to 0$. In practice the best fit to the data is obtained

with $\omega = 0.99$, and the value of p(1), the pressure at which S = 1, gives a value of $Q_g = 2.1 \times 10^{-17}$cm . If we assume a value of $Q_m = 3 \times 10^{-16}$cm^2 for He at this energy, then our data gives $\Sigma Q_x = 1.4 \times 10^{-18}$cm^2, when in fact it should give $\Sigma Q_x = 0$. The above numbers are to be regarded as "background noise" of unknown origin below which we cannot expect to measure. As we shall see the present data in N_2 and O_2 yield much larger values of ΣQ_x than the background limit given above, and there appears to be no reason to doubt the interpretation of data such as that in Fig. 9, in terms of the effects of inelastic collisions.

Having established satisfactory self-consistency of data such as that in Fig. 9, and the close agreement in shape between the theoretical curves and the data, the electron energy dependence of Q_g was measured at a number of pressures by taking $z\text{-}y_1\text{-}y_2$ plots $I^+(C_1)$ and $I^+(C_3)$ versus electron accelerating voltage. The ratio $I^+(C_1)/I^+(C_3)$ was then computed at suitably spaced points and the value of S obtained therefrom by reference to a theoretical curve such as that plotted in Fig. 9. The use of Eq. 14 together with the known pressure then yields Q_g at each point treated.

The results of such measurements in N_2 are shown in Fig. 11 where the various symbols refer to different runs taken with a number of different pressures of nitrogen and with different partial pressures, including zero, of NO. The latter was always small and the amount used was found not to affect the results. Its presence, however, allowed the measurements to be extended downwards in energy from the ionization potential of N_2, 15.6 eV, to close to that of NO, 9.25 eV.

The data on Q_g is to be regarded as the primary data obtained from this type of experiment. Further interpretation to obtain ΣQ_x can be performed without mathematical difficulty, as outlined in the preceding section, but does require a knowledge of the momentum transfer cross-section Q_m. Any error in the value of Q_m used is carried through

in inverse proportion as an error in ΣQ_x, as is obvious from Eq. 15. We may also note that the percentage error in Q_g is doubled on converting to ΣQ_x.

The primary data on Q_g has been converted to ΣQ_x in the lower half of Fig. 11 using for Q_m the curve shown, which is that given by Engelhardt, Phelps and Risk[21] who found it compatible with their analysis of electron transport coefficients in N_2. Such an analysis is sensitive to Q_m at electron energies below a few volts, but becomes decreasingly sensitive with increasing energy. Hence, in the region of present interest the Q_m data is of unknown accuracy. It is to be hoped that in the future more accurate values of Q_m become available allowing the Q_g data to be reanalyzed to give more accurate data on ΣQ_x.

Measurements of ion current ratios have also been conducted in O_2 using the same procedures as described above. The data so obtained are summarized in Fig. 12 where once agin Q_g is to be regarded as the primary data. In the lower half of the figure the energy dependence of ΣQ_x has been deduced assuming the momentum transfer cross-section shown. This is an average of the two shpaes obtained with and without an assumed resonance at 4.5 eV, by Hake and Phelps[22] in their analysis of measured electron transport coefficients in O_2. Similar remarks apply regarding its reliability, and consequently the reliability of the ΣQ_x curve, as were made with regard to N_2 above.

Measurement of Q_g using Negative Ion Production

In order to extend the data on Q_g to lower electron energies an attempt was made to employ negative ion current ratio measurement in an analogous fashion to that used with positive ionization, as described above. In principle, by the addition of suitably small partial pressures of, for example O_2 and NO to N_2 it should be possible to cover

---

21) A. G. Engelhardt, A. V. Phelps, and C. G. Risk, Phys. Rev, 135, A1566 (1964).

22) R. D. Hake and A. V. Phelps, Phys. Rev. 158, 70 (1967).

the energy range from approximately 5 eV to 10 eV, and thereby overlap the positive ion data of Fig. 11. Similarly, such data should be obtainable in O_2 by the addition of NO.

Attempts to obtain useful data of this type, in both N_2 and O_2, were unfortuantely frustrated by problems which appear to be insurmountable with the present apparatus. Firstly, the use of O_2 and NO, added to N_2 in low enough partial pressures not to affect the electron scattering, gave negative ion signals which were too small to be distinguished accurately from a negative background current, presumably scattered electrons, reaching $C_{1,2,3}$ at the higher pressures. As a result of this the pressure dependence of the negative ion current ratios did not follow the theoretical curves, as they did with the positive ion data an example of which is shown in Fig. 9. This problem could be solved by mass-analysis of the sampled negative current but such measurements would require a completely redesigned experimental system. Negative ion current ratio measurements were somewhat more successful in pure O_2 where at low energies, in the region of 6 eV, data of the type shown in Fig. 9 did give a reasonable fit to the theoretically predicted shape. However, data taken at higher energies, with or without added NO, were not consistent with theory, presumably due to similar problems of collection of scattered electrons by $C_{1,2,3}$.

In view of these problems no data on the measurement of Q_g can be reported from the negative ion work conducted during the latter part of the contract.

3. RECOMMENDATIONS FOR FUTURE WORK

3.1

The usefulness of the present measurements of the momentum transfer cross-section Q_m in N_2, and of the cross-section Q_g in N_2 and O_2 would be markedly increased if work were performed to investigate the extent to which the present measurements of Q_m are being falsified by reflection of back-scattered electrons at the entrance plate boundary of the scattering chamber. Methods for carrying out such a study have been suggested in Ref. 20.

3.2

The extension of the preliminary work reported here on attachment to SF_4 at various temperatures is desirable, including an investigation of which fragment ions are to be ascribed to the SOF_2 impurity.

4. PUBLICATIONS AND PRESENTATIONS SINCE SEPTEMBER 1, 1969

The following is a list of publications describing work performed under the current or previous related contracts which have appeared in various scientific publications since September 1, 1969. Also shown are the titles of oral presentations which have been made.

(i) "Temperature Dependence of Dissociative Attachment in N_2O" by P. J. Chantry, J. Chem Phys. 51, 3369 (1969).

(ii) "Formation of N_2O^- via Ion-Molecule Reactions in N_2O" by P. J. Chantry, J. Chem. Phys. 51, 3380 (1969).

(iii) "Spurious Dissociative Attachment Peaks from Inelastic Energy Loss Reactions", by P. J. Chantry, Bull. Amer. Phys. Soc. II15, 418 (1970).

(iv) "Temperature Dependence of SF_6^-, SF_5^-, and F^- Production From SF_6", by C. L. Chen and P. J. Chantry, Bull. Amer. Phys. Soc. II15, 418 (1970).

Items (iii) and (iv) are abstracts of oral presentations made at the 22nd Gaseous Electronics Conference, Gatlinburg, Tennessee, 1969.

REFERENCES

1. Annual Report, Contract DAHC04-69-C-0094, submitted April 1970.
2. MKS Instruments, Burlington, Mass.
3. G. Herzberg, Molecular Spectra and Molecular Structure III. (D. Van Nostrand, Inc., New York, 1966).
4. L. M. Branscomb, D. S. Burch, S. J. Smith, and S. Geltman, Phys. Rev. 111 504 (1958).
5. J. L. Pack and A. V. Phelps, J. Chem. Phys. 44, 870, 1966.
6. P. J. Chantry, J. Chem. Phys. 51 3369 (1969).
7. R. K. Durran, J. Chem. Phys. 35, 1849 (1961).
8. D. Stelman and A. V. Phelps, Final Report, Contract F29601-68-C-0070, June. 1969.
9. R. L. Wilkins, J. Chem. Phys. 51, 853 (1969).
10. C. L. Chen and P. J. Chantry, Bull Amer. Phys. Soc. II 15, 418 (1970). See also Final Report, Contract N00014-68-C-0490, Sept., 1969.
11. Matheson Company Inc., East Rutherford, New Jersey.
12. P. J. Chantry, A. V. Phelps, and G. J. Schulz, Phys. Rev. 152, 81 (1966).
13. I. W. Busbridge and S. E. Orchard, Astrophys. J. 149, 655 (1967).
14. S. E. Orchard Astrophys J. 149, 665 (1967).
15. H. C. van de Hulst and K. Grossman, The Atmospheres of Venus and Mars, ed J. C. Brandt and M. B. McElroy, (Gordon and Breach, New York, 1968) p. 35.
16. See for example S. Chandrasekhar Radiative Transfer (Clarendon Press, Oxford, England, 1950).

17. See ref. 16, p. 19.

18. B. Davison, Neutron Transport Theory (Clarendon Press, Oxford, England, 1957), p. 55.

19. J. E. Hansen, Astrophys. J. 158, 337 (1969).

20. P. J. Chantry, Proposal for continuation of Contract DAHC04-69-C-0094.

21. A. G. Engelhardt, A. V. Phelps, and C. G. Risk, Phys. Rev, 135, A1566 (1964).

22. R. D. Hake and A. V. Phelps, Phys. Rev. 158, 70 (1967).

FIGURE CAPTIONS

Fig. 1 - The variable temperature collision chamber apparatus used in the ozone measurements, showing the electron beam (EB), the attractor (Attr) and repeller (Rep) plates and the internal thermocouple (TC).

Fig. 2 - The attachment cross sections in ozone. The peak total cross section (Q_a) is $(3.0 \pm \frac{0.7}{0.4}) \times 10^{-17}$ cm^2. The shapes and relative magnitudes of the cross sections for O^- and O_2^- production were determined mass spectrometrically as described in the text. The sum of these agrees with the measured total cross section below 1.2 eV, and is indicated by the broken curve at higher energies. The broken curve below 0.5 eV is the adjustment of the total cross section required to give agreement with swarm measurements.

Fig. 3 - Kinetic energy spectra of O^- ions produced from O_3 by electrons at the energies indicated. The smooth curves have been drawn through data points, shown only on the lowest curve. Similar scatter exists on all curves. The curves are normalized to give the same peak height at zero energy.

Fig. 4 - The electron energy dependence of the high kinetic energy peaks observed for O^- and O_2^-. See figure 3. The points represent the position of the peak. The broken lines are plots of Eq. (3) and indicate the position of the points expected if all the excess energy were released as kinetic energy.

Fig. 5 - Relative SF_4^- and SF_3^- signals observed at low electron energies and room temperature in SF_4. The width of the SF_4^- peak is determined by the available energy resolution (0.08 eV FWHM). Its magnitude has been reduced by a factor of 10^3 in order to show it on the same scale as the SF_3^- signal.

Fig. 6 - The high pressure electron beam tube, showing the Baratron pressure gauge (Bar), electron collectors (EC), ion collectors $C_{1,2,3}$, gas reservoirs ($G_{1,2}$) and leak valves (LV).

Fig. 7 - The correction factor β appearing in Eq. 15, $\Sigma Q_x = \beta Q_g^2/Q_m$, plotted as a function of Q_g/Q_m. Also shown for reference is the relationship between $\Sigma Q_x/Q_m$ and Q_g/Q_m.

Fig. 8 - The momentun transfer (Q_m) and total (Q_T) cross sections in N_2. The curve labelled EPR is from ref. 21. See discussion in text regarding the discrepancies.

Fig. 9 - Pressure dependence of the positive ion current ratios measured in N_2 at 17 eV. The points are experimental, the full curves are theoretically computed using $\omega = 0.9$ and assuming no electron reflection at the boundaries. Their lateral positions are adjusted for best fit and yield the pressures at which S = 1, shown by the vertical bar on each curve.

Fig. 10 - Pressure dependence of the positive ion current ratio $I^+(C_1)/I^+(C_3)$ measured in He, with a small partial pressure of NO added, at 18 eV. See text for discussion.

Fig. 11 - The energy dependence of the measured "cross-section" Q_g in N_2, and the behavior of the total inelastic collision cross-section ΣQ_x, deduced from Q_g using the momentum transfer cross-section Q_m shown, obtained from ref. 21.

Fig. 12 - The energy dependence of the measured "cross-section" Q_g in O_2, and the behavior of the total inelastic collision cross-section ΣQ_x deduced from Q_g using the momentum transfer cross-section Q_m shown, obtained from ref. 22.

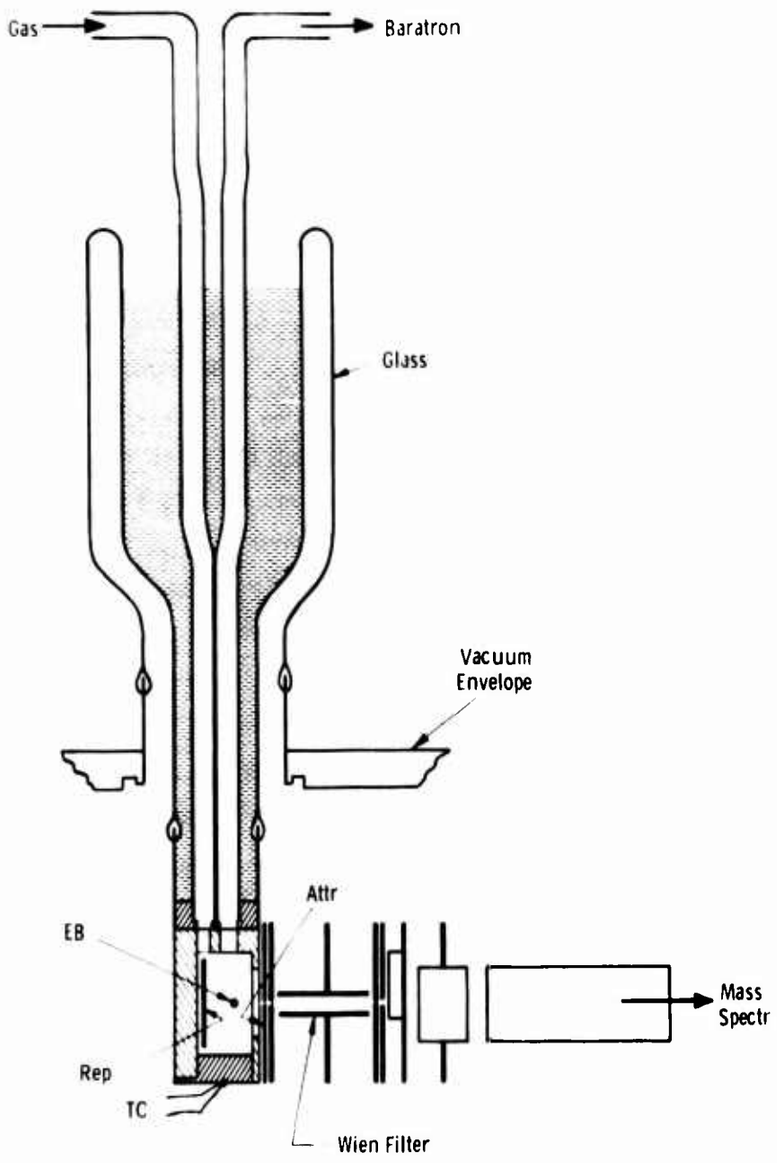

Fig. 1 - The variable temperature collision chamber apparatus used in the ozone measurements, showing the electron beam (EB), the attractor (Attr) and repeller (Rep) plates and the internal thermocouple (TC).

Curve 586/40-A

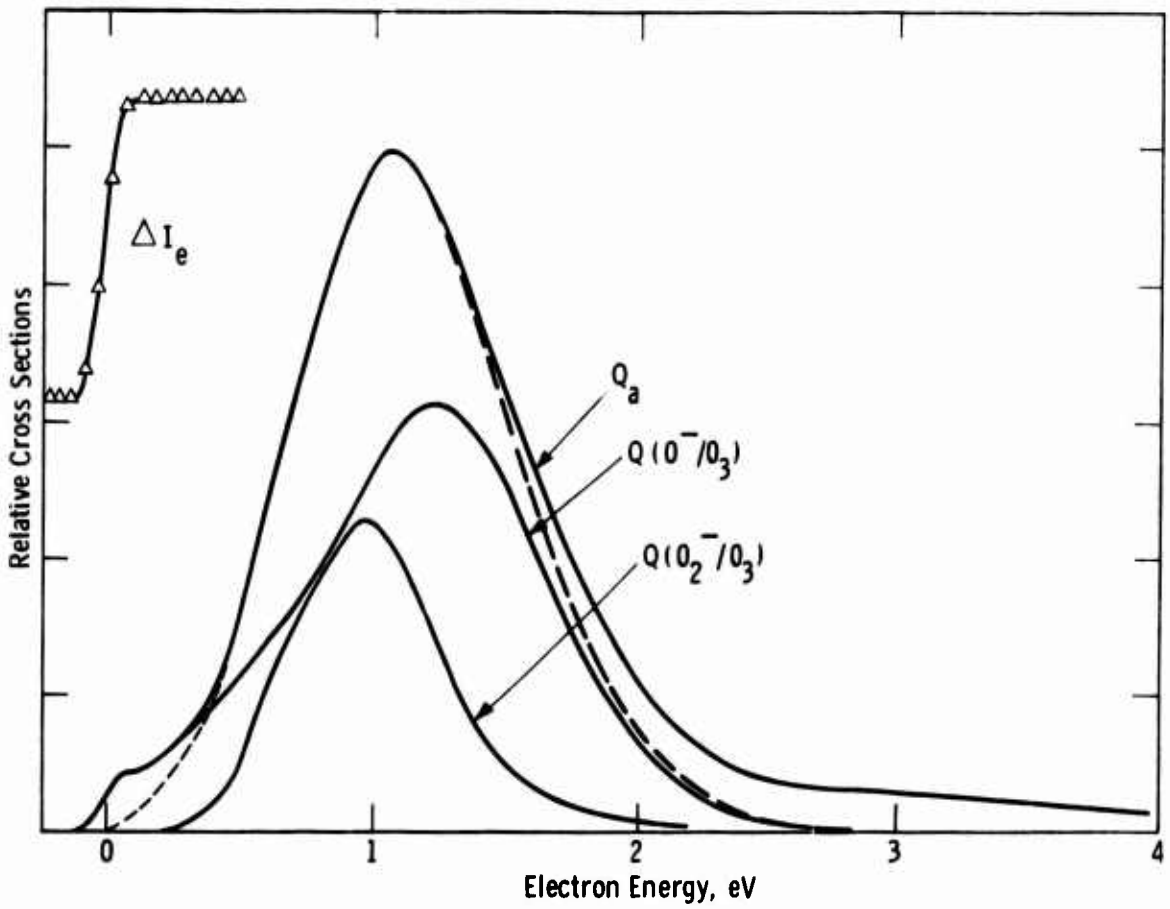

Fig. 2 - The attachment cross sections in ozone. The peak total cross section (Q_a) is $(3.0 \pm {}^{0.7}_{0.4}) \times 10^{-17}$ cm^2. The shapes and relative magnitudes of the cross sections for O^- and O_2^- production were determined mass spectrometrically as described in the text. The sum of these agrees with the measured total cross section below 1.2 eV, and is indicated by the broken curve at higher energies. The broken curve below 0.5 eV is the adjustment of the total cross section required to give agreement with swarm measurements.

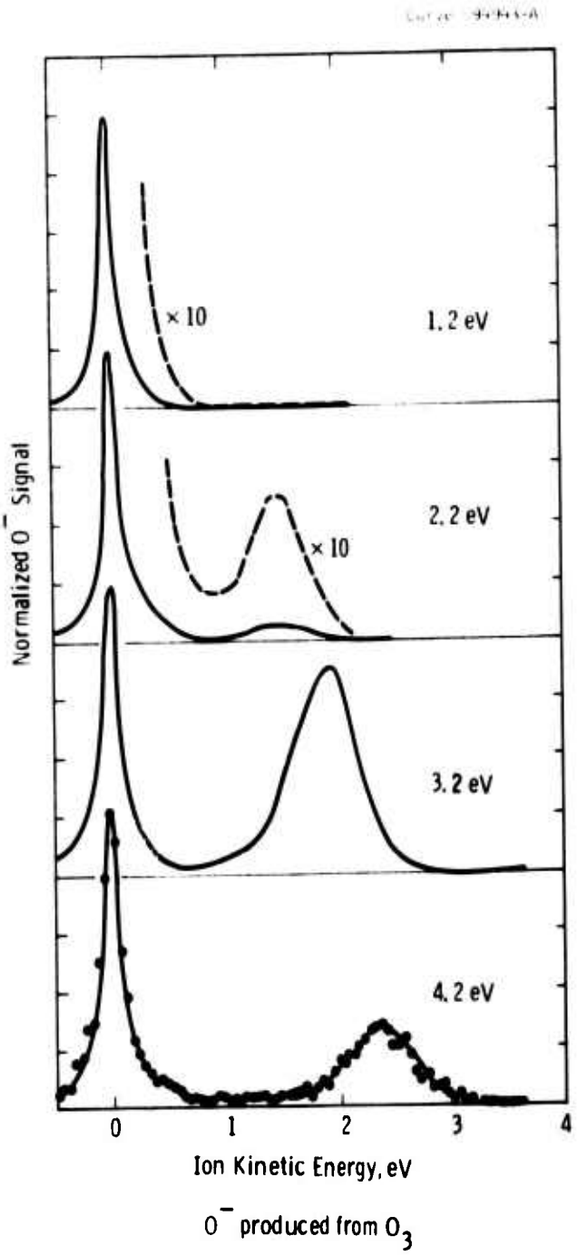

Fig. 3 - Kinetic energy spectra of O^- ions produced from O_3 by electrons at the energies indicated. The smooth curves have been drawn through data points, shown only on the lowest curve. Similar scatter exists on all curves. The curves are normalized to give the same peak height at zero energy.

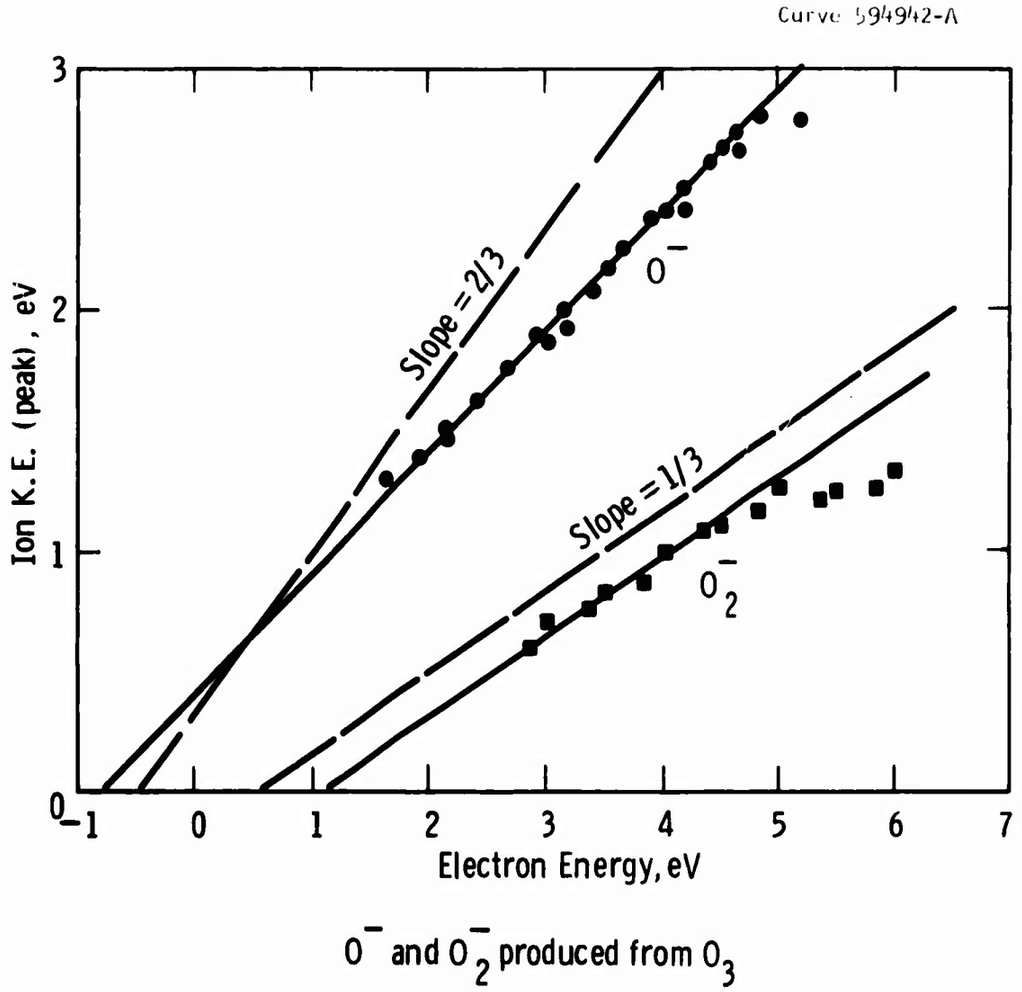

O^- and O_2^- produced from O_3

Fig. 4 - The electron energy dependence of the high kinetic energy peaks observed for O^- and O_2^-. See figure 3. The points represent the position of the peak. The broken lines are plots of Eq. (3) and indicate the position of the points expected if all the excess energy were released as kinetic energy.

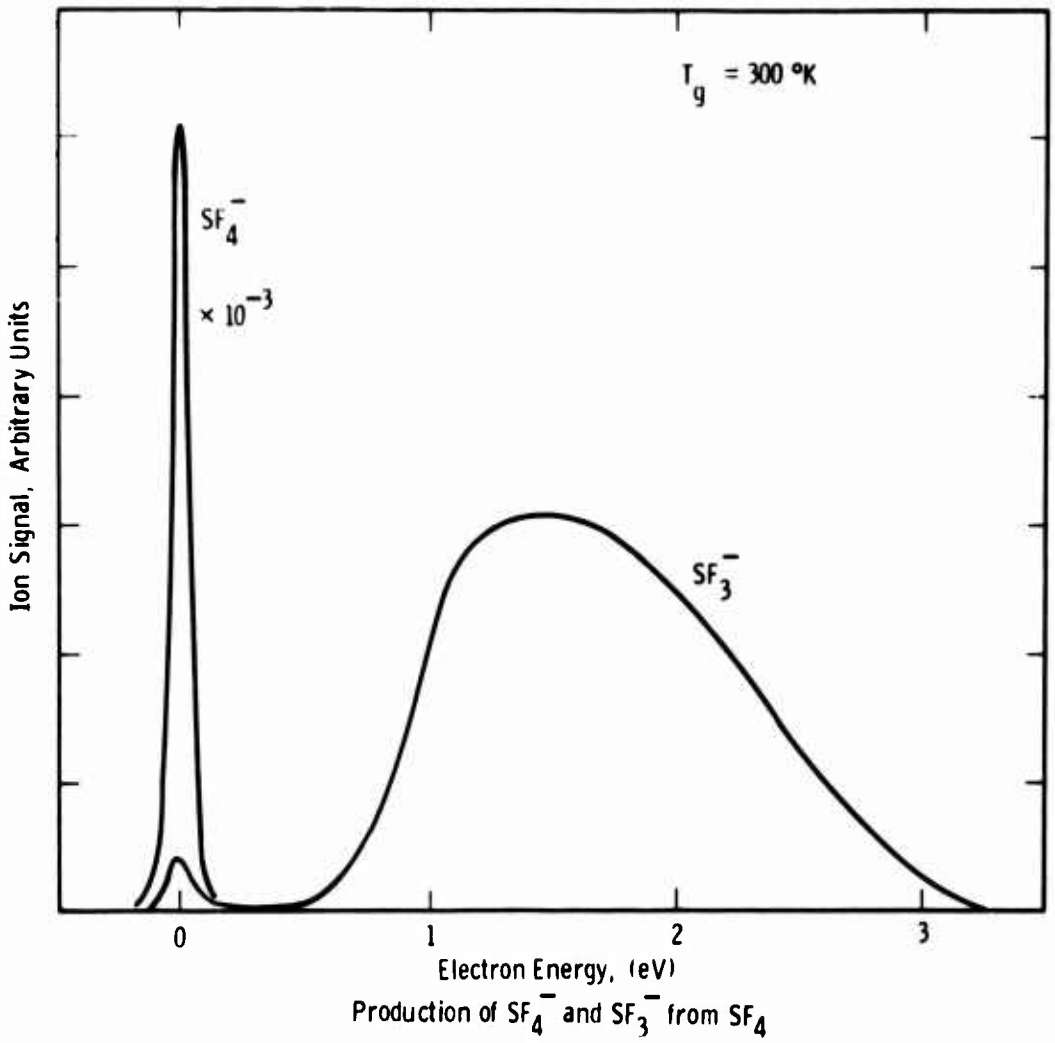

Fig. 5 - Relative SF_4^- and SF_3^- signals observed at low electron energies and room temperature in SF_4. The width of the SF_4^- peak is determined by the available energy resolution (0.08 eV FWHM). Its magnitude has been reduced by a factor of 10^3 in order to show it on the same scale as the SF_3^- signal.

Dwg. 2918A25

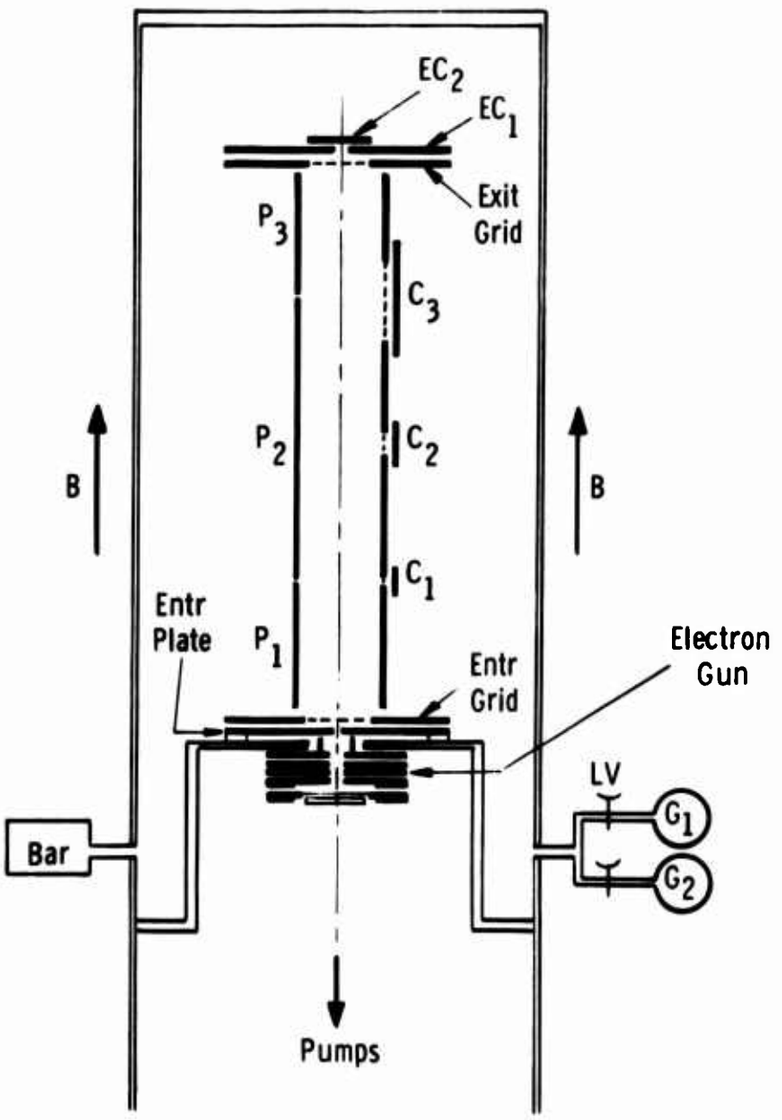

Fig. 6 - The high pressure electron beam tube, showing the Baratron pressure gauge (Bar), electron collectors (EC), ion collectors $C_{1,2,3}$, gas reservoirs ($G_{1,2}$) and leak valves (LV).

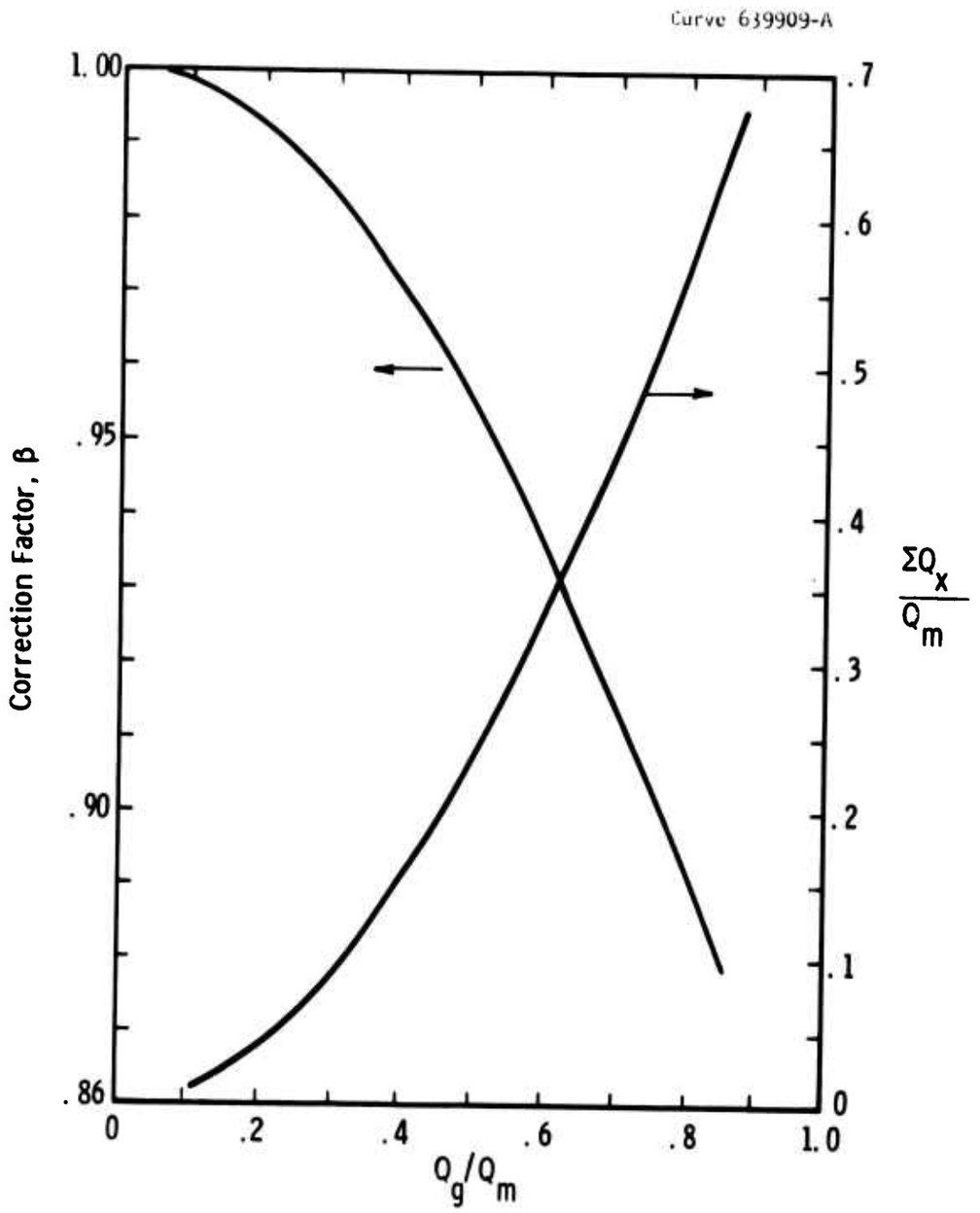

Fig. 7 - The correction factor β appearing in Eq. 15, $\Sigma Q_x = \beta Q_g^2/Q_m$, plotted as a function of Q_g/Q_m. Also shown for reference is the relationship between $\Sigma Q_x/Q_m$ and Q_g/Q_m.

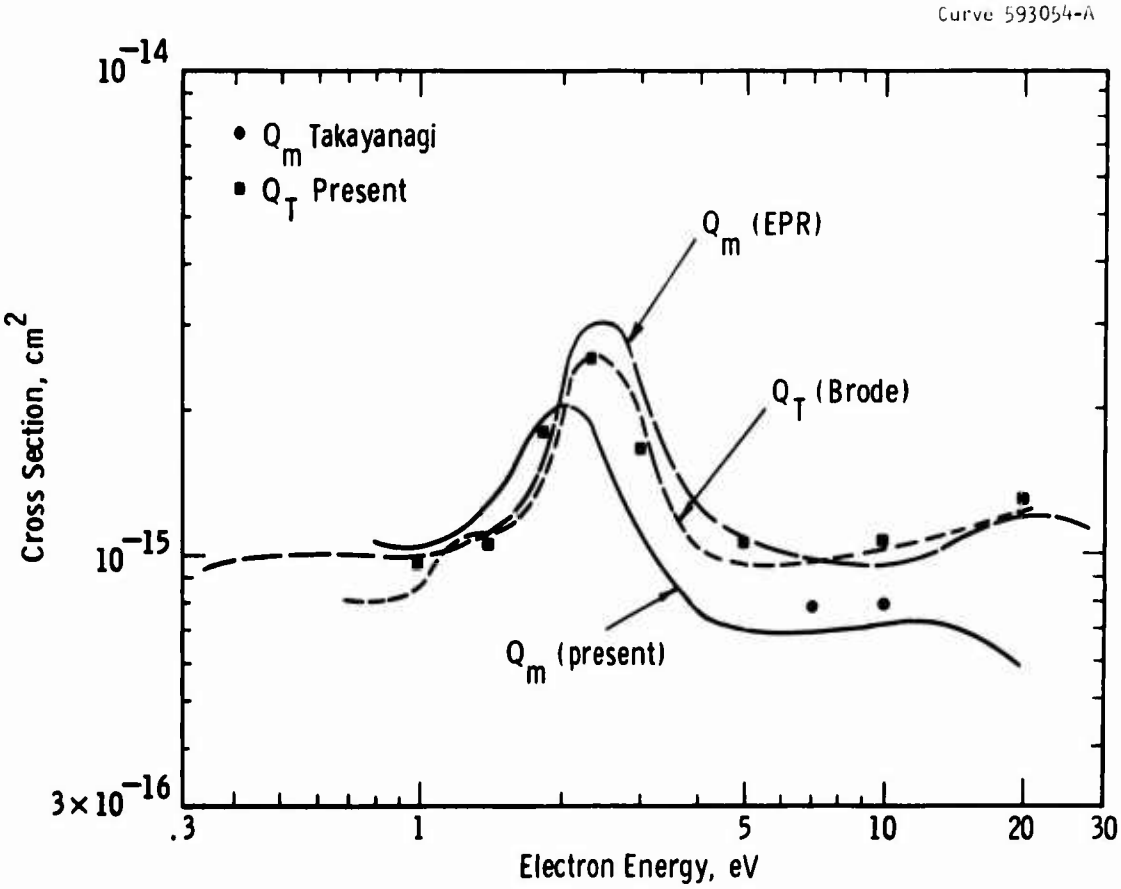

Fig. 8 - The momentum transfer (Q_m) and total (Q_T) cross sections in N_2. The curve labelled EPR is from Ref. 21. See discussion in text regarding the discrepancies.

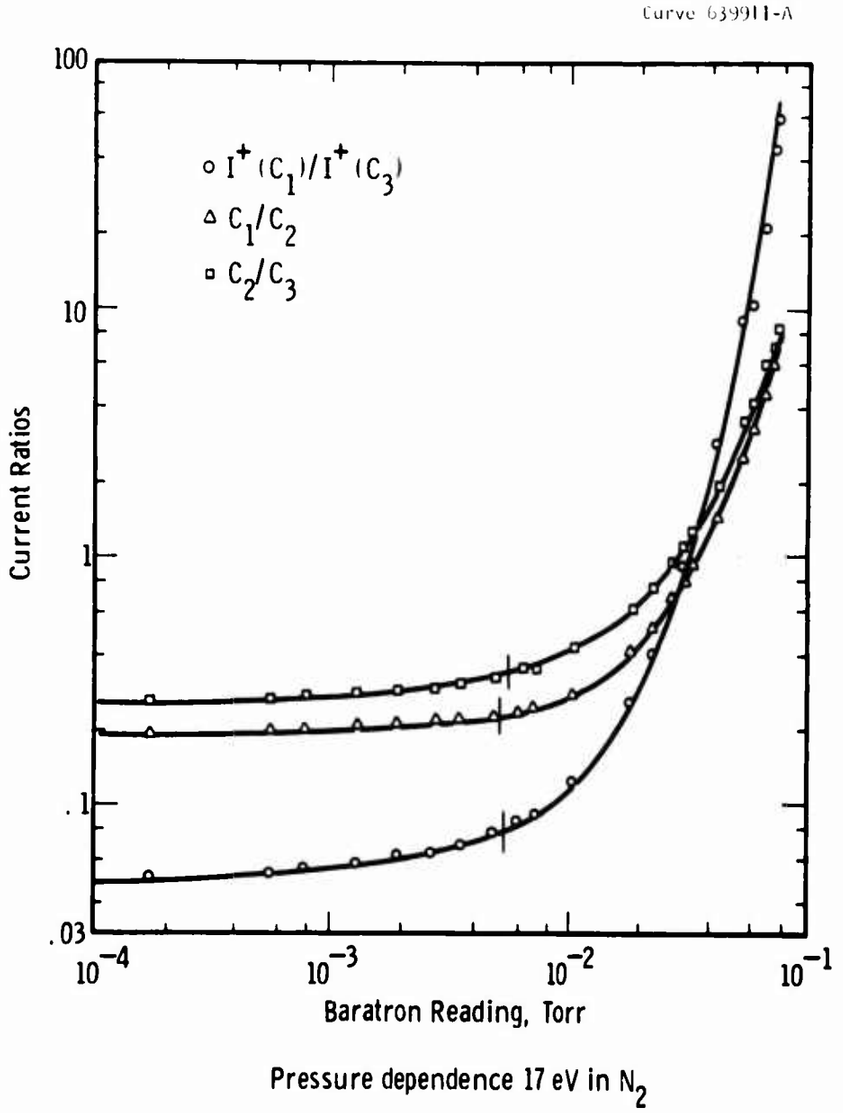

Fig. 9 - Pressure dependence of the positive ion current ratios measured in N_2 at 17 eV. The points are experimental, the full curves are theoretically computed using $\omega = 0.9$ and assuming no electron reflection at the boundaries. Their lateral positions are adjusted for best fit and yield the pressures at which S = 1, shown by the vertical bar on each curve.

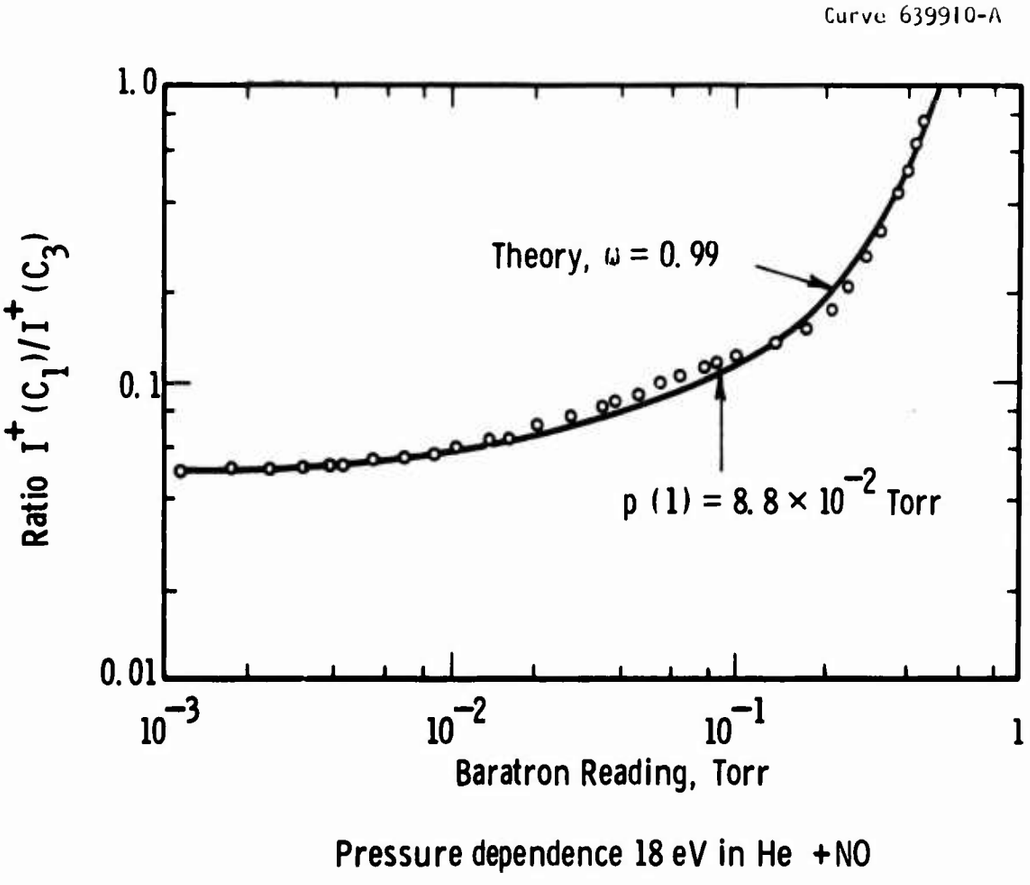

Fig. 10 - Pressure dependence of the positive ion current ratio $I^+(C_1)/I^+(C_3)$ measured in He, with a small partial pressure of NO added, at 18 eV. See text for discussion.

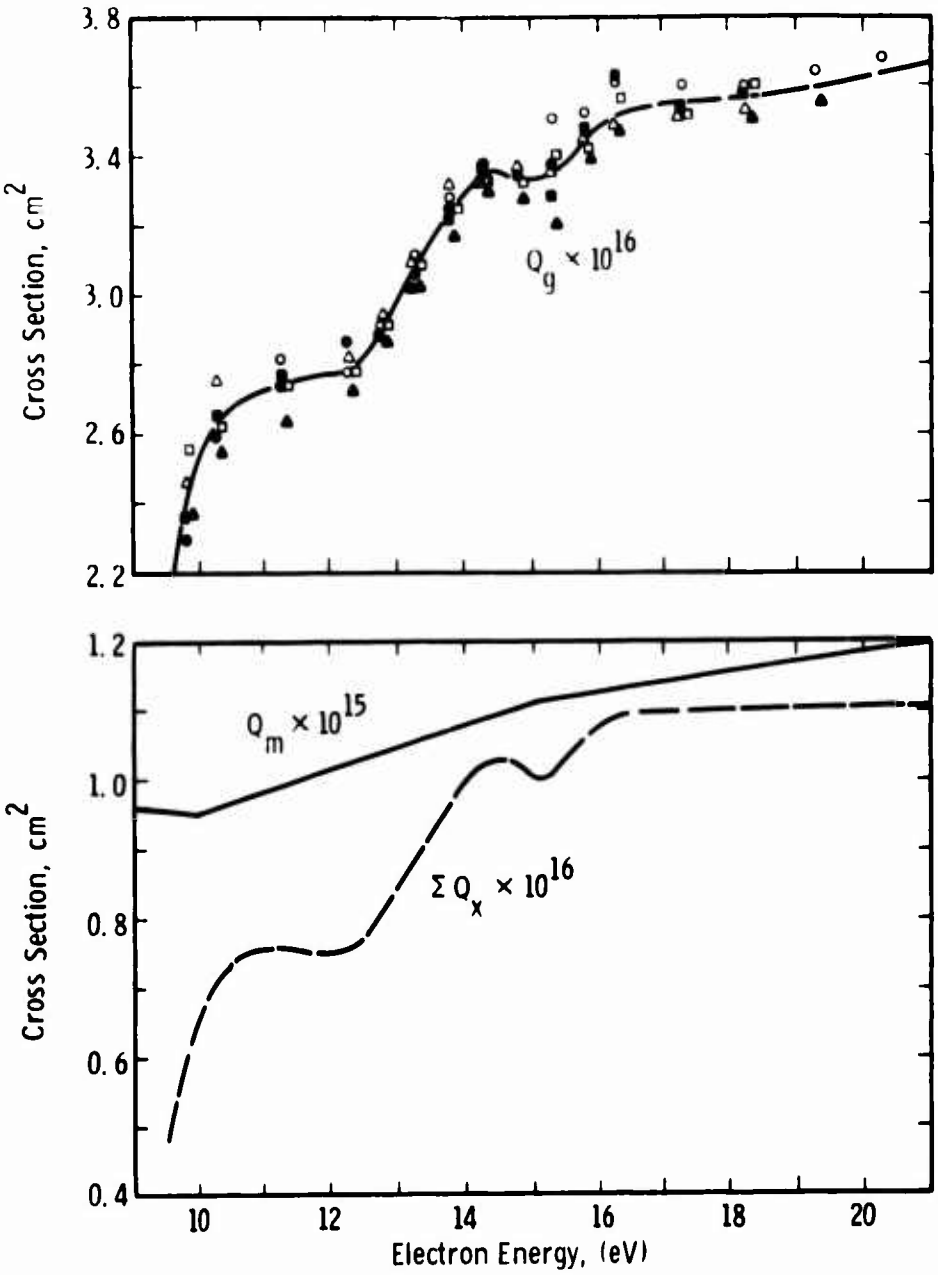

Cross-sections in nitrogen

Fig. 11 - The energy dependence of the measured "cross-section" Q_g in N_2, and the behavior of the total inelastic collision cross-section ΣQ_x, deduced from Q_g using the momentum transfer cross-section Q_m shown, obtained from ref. 21.

Curve 649912-A

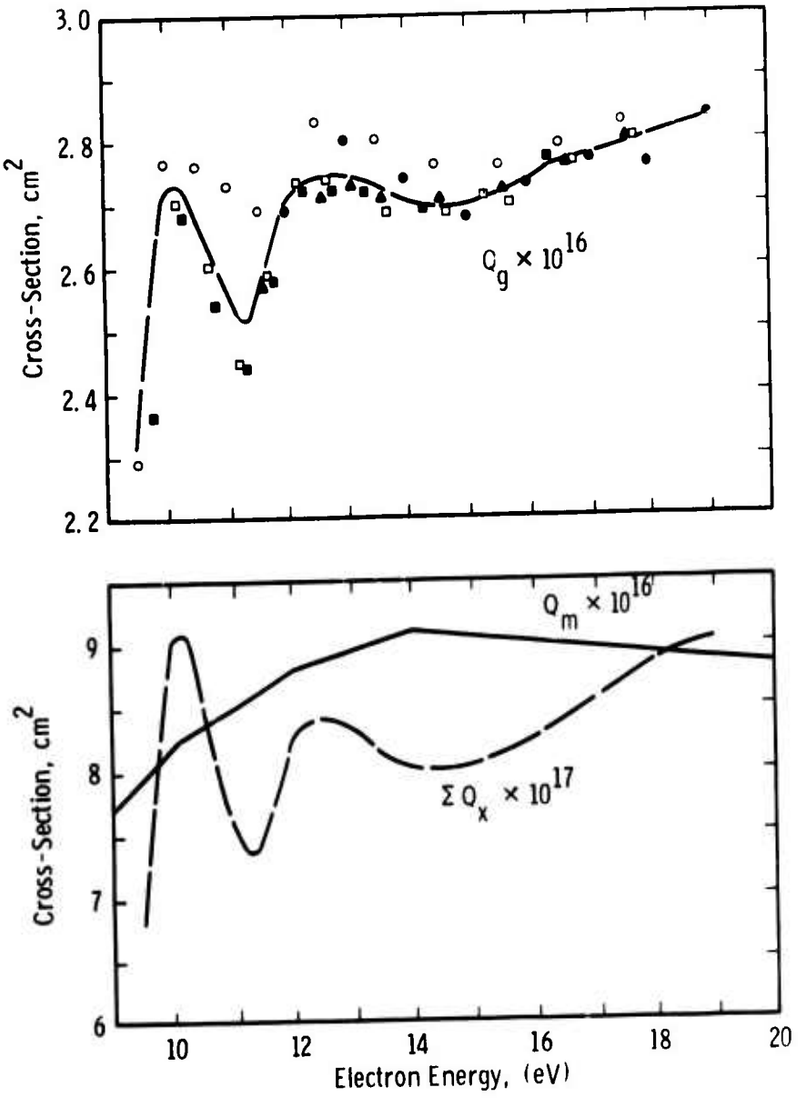

Cross-sections in oxygen

Fig. 12 - The energy dependence of the measured "cross-section" Q_g in O_2, and the behavior of the total inelastic collision cross-section ΣQ_x deduced from Q_g using the momentum transfer cross-section Q_m shown, obtained from ref. 22.

Unclassified

Security Classification

DOCUMENT CONTROL DATA - R & D

(Security classification of title, body of abstract and indexing annotation must be entered when the overall report is classified)

1. ORIGINATING ACTIVITY (Corporate author) Westinghouse Electric Corporation	2a. REPORT SECURITY CLASSIFICATION Unclassified 2b. GROUP NA

3. REPORT TITLE

Atomic Collision Processes Relating to the Ionosphere

4. DESCRIPTIVE NOTES (Type of report and inclusive dates)

Final Report: 1 September 1969 - 31 August 1970

5. AUTHOR(S) (First name, middle initial, last name)

P. J. Chantry
A. V. Phelps

6. REPORT DATE	7a. TOTAL NO. OF PAGES	7b. NO. OF REFS
1970	39	22

8a. CONTRACT OR GRANT NO. DAHC04 69 C 0094 b. PROJECT NO. c. d.	9a. ORIGINATOR'S REPORT NUMBER(S) NA 9b. OTHER REPORT NO(S) (Any other numbers that may be assigned this report) 8829.1-P

10. DISTRIBUTION STATEMENT

This document has been approved for public release and sale; its distribution is unlimited.

11. SUPPLEMENTARY NOTES	12. SPONSORING MILITARY ACTIVITY
	U. S. Army Research Office-Durham Box CM, Duke Station Durham, North Carolina 27706

13. ABSTRACT

Measurements of the attachment cross-sections in O_3 reveal no dependence on temperature below 360°K in the energy range 0-4 eV. The peak value of the total attachment cross-section Q_a, of $(3.0 \pm \begin{smallmatrix}0.7\\0.4\end{smallmatrix}) \times 10^{-17}$ cm^2 occurs at an electron energy of 1.07 eV. The individual cross-sections for production of O^- and O_2^- peak at energies of 1.25 eV and 0.95 eV respectively. The ratios of the three cross-sections Q_a:$Q(O^-)$: $Q(O_2^-)$ at their peaks are 1.6:1:0.75. From the measured onset for O_2^- production a value of $A(O_2) \geq 0.60 \pm \begin{smallmatrix}0.05\\0.15\end{smallmatrix}$ eV is deduced for the electron affinity of O_2.

14. KEY WORDS

Ozone - Electron Attachment
Inelastic Collision Cross-sections
Atomic Collision Processes

DD FORM 1 NOV 65 1473 REPLACES DD FORM 1473, 1 JAN 64, WHICH IS OBSOLETE FOR ARMY USE.

Unclassified